Nuclear energy density functional from chiral two- and three-nucleon interactions[1]

J.W. Holt, N. Kaiser and W. Weise

Physik Department, Technische Universität München, D-85747 Garching, Germany

email: nkaiser@ph.tum.de

Abstract

An improved density-matrix expansion is used to calculate the nuclear energy density functional from chiral two- and three-nucleon interactions. The two-body interaction comprises long-range one- and two-pion exchange contributions and a set of contact terms contributing up to fourth power in momenta. In addition we employ the leading order chiral three-nucleon interaction with its parameters c_E, c_D and $c_{1,3,4}$ fixed in calculations of nuclear few-body systems. With this input the nuclear energy density functional is derived to first order in the two- and three-nucleon interaction. We find that the strength functions $F_\nabla(\rho)$ and $F_{so}(\rho)$ of the surface and spin-orbit terms compare in the relevant density range reasonably with results of phenomenological Skyrme forces. However, an improved description requires (at least) the treatment of the two-body interaction to second order. This observation is in line with the deficiencies in the nuclear matter equation of state $\bar{E}(\rho)$ that remain in the Hartree-Fock approximation with low-momentum two- and three-nucleon interactions.

PACS: 12.38.Bx, 21.30.Fe, 21.60.-n, 31.15.Ew
Keywords: Nuclear energy density functional; Density-matrix expansion; Chiral two- and three-nucleon interactions

arXiv:1107.5966v1 [nucl-th] 29 Jul 2011

1 Introduction

The nuclear energy density functional approach is the many-body method of choice in order to calculate the properties of medium-mass and heavy nuclei in a systematic manner [1, 2]. Parameterized non-relativistic Skyrme functionals [3, 4] as well as relativistic mean-field models [5, 6] have been widely and successfully used for such nuclear structure calculations. A complementary approach [7, 8, 9, 10] focuses less on the fitting of experimental data, but attempts to constrain the analytical form of the functional and the values of its couplings from many-body perturbation theory and the underlying two- and three-nucleon interaction. Switching from conventional hard-core NN-potentials to low-momentum interactions [11, 12] is essential in this respect, because the nuclear many-body problem formulated in terms of the latter becomes significantly more perturbative. Indeed, second-order perturbative calculations including also three-body forces give already a good account of the bulk correlations in infinite nuclear matter [13, 14] and in doubly-magic nuclei [15].

In many-body perturbation theory the contributions to the energy are written in terms of density-matrices convoluted with the finite-range interaction kernels, and are therefore highly non-local in both space and time. In order to make such functionals numerically tractable in heavy open-shell nuclei it is desirable to develop simplified approximations for these functionals in terms of local densities and currents only. In such a construction the density-matrix expansion comes prominently into play as it removes the non-local character of the exchange

[1]Work supported in part by BMBF, GSI and the DFG cluster of excellence: Origin and Structure of the Universe.

(Fock) contribution to the energy by mapping it onto a generalized Skyrme functional with density-dependent couplings. For some time the prototype for that has been the density-matrix expansion of Negele and Vautherin [16], but recently Gebremariam, Duguet and Bogner [17] have developed an improved version for spin-unsaturated nuclei. They have demonstrated that phase-space averaging techniques allow for a consistent expansion of both the spin-independent (scalar) part as well as the spin-dependent (vector) part of the density-matrix. The improved properties of the new phase-space averaged density-matrix expansion have been extensively studied via the Fock energy densities arising from schematic finite-range central, tensor and spin-orbit interactions for a large set of semi-magic nuclei (for further details see ref.[17]).

In order to match with these new developments, the nuclear energy density functional as it emerges from chiral pion-nucleon dynamics has been recalculated in ref.[18]. This calculation has treated for isospin-symmetric (i.e. $N = Z$) nuclear systems the effects from 1π-exchange, iterated 1π-exchange, and irreducible 2π-exchange with intermediate Δ-isobar excitations, including Pauli-blocking corrections up to three-loop order. Among other things, it has been found that the two- and three-body contributions to the spin-orbit coupling strength $F_{so}(\rho)$, as generated by 2π-exchange, tend to cancel each other in the relevant density range $\rho \simeq 0.08\,\mathrm{fm}^{-3}$, thus leaving room for the short-range nuclear spin-orbit interaction. The short-range components of the NN-interaction together with the constraints on them provided by the elastic scattering data (i.e. NN-phase shifts etc.) have not been considered explicitly in ref.[18]. Furthermore, a similar calculation of a microscopically constrained nuclear energy density functional derived from the chiral NN-potential at next-to-next-to-leading order ($\mathrm{N^2LO}$) has been presented recently by Gebremariam, Bogner and Duguet in ref.[19]. They have proposed that the density-dependent couplings associated with the pion-exchange interactions should be added to a standard Skyrme functional (with several adjustable parameters). In the sequel it has been demonstrated in ref.[20] that this new energy density functional gives numerically stable results and that it exhibits a small but systematic reduction of the χ^2-measure compared to standard Skyrme functionals (without any pion-exchange terms).

The purpose of the present paper is to derive a nuclear energy density functional with improved (chiral) two- and three-nucleon interactions. We use for the two-body interaction the $\mathrm{N^3LO}$ chiral NN-potential which reaches at this order the quality of a high-precision NN-potential (in reproducing empirical NN-shifts and deuteron properties). The $\mathrm{N^3LO}$ chiral potential consists of long-range one- and two-pion exchange terms and two dozen low-energy constants which parameterize the short-distance part of the NN-interaction. The latter contact potential written in momentum space gives the most general contribution up to fourth power in momenta. In the actual calculation we will use the version $\mathrm{N^3LOW}$ of the chiral NN-potential developed in refs.[21, 22] by lowering the cut-off scale to $\Lambda = 414\,\mathrm{MeV}$. This value coincides with the resolution scale inherent to the universal low-momentum NN-potential $V_{\mathrm{low-k}}$ [11, 12] to which all realistic NN-potentials flow after integrating out effects from momenta above the cut-off scale $\Lambda = 2.1\,\mathrm{fm}^{-1}$. The low-momentum two-body interaction $\mathrm{N^3LOW}$ is supplemented by the leading order chiral three-nucleon interaction with its parameters c_E, c_D and $c_{1,3,4}$ determined in calculations of nuclear few-body systems [13, 23]. Our paper is organized as follows. In section 2 we recall the basic features of the (improved) density-matrix expansion and the nuclear energy density functional for isospin-symmetric systems. In section 3 we present the two-body contributions to the various density-dependent strength functions $\bar{E}(\rho)$, $F_\tau(\rho)$, $F_d(\rho)$, $F_{so}(\rho)$ and $F_J(\rho)$, separately for the finite-range pion-exchange and the zero-range contact interactions. In section 4, we collect the corresponding analytical expressions for the three-body contributions grouped into contact (c_E), 1π-exchange (c_D) and 2π-exchange ($c_{1,3,4}$) terms. Section 5 is devoted to the discussion of our numerical results and sections 6 ends with a summary and an outlook.

2 Density-matrix expansion and energy density functional

The starting point for the construction of an explicit nuclear energy density functional is the density-matrix as given by a sum over the energy eigenfunctions $\Psi_\alpha(\vec{r}\,)$ representing occupied orbitals of the (non-relativistic) many-fermion system. According to Gebremariam, Duguet and Bogner [17] it can be expanded in relative and center-of-mass coordinates, $\vec{a}$ and $\vec{r}$, as follows:

$$\begin{aligned}\sum_\alpha \Psi_\alpha(\vec{r}-\vec{a}/2)\Psi^\dagger_\alpha(\vec{r}+\vec{a}/2) &= \frac{3\rho}{ak_f}\,j_1(ak_f) - \frac{a}{2k_f}\,j_1(ak_f)\Big[\tau - \frac{3}{5}\rho k_f^2 - \frac{1}{4}\vec{\nabla}^2\rho\Big] \\ &\quad + \frac{3i}{2ak_f}\,j_1(ak_f)\,\vec{\sigma}\cdot(\vec{a}\times\vec{J}) + \dots\,, \end{aligned} \tag{1}$$

with the spherical Bessel function $j_1(x) = (\sin x - x\cos x)/x^2$. The quantities appearing on the right hand side of eq.(1) are: the (local) nucleon density $\rho(\vec{r}\,) = 2k_f^3(\vec{r}\,)/3\pi^2 = \sum_\alpha \Psi^\dagger_\alpha(\vec{r}\,)\Psi_\alpha(\vec{r}\,)$, the (local) kinetic energy density $\tau(\vec{r}\,) = \sum_\alpha \vec{\nabla}\Psi^\dagger_\alpha(\vec{r}\,)\cdot\vec{\nabla}\Psi_\alpha(\vec{r}\,)$ and the (local) spin-orbit density $\vec{J}(\vec{r}\,) = i\sum_\alpha \vec{\Psi}^\dagger_\alpha(\vec{r}\,)\vec{\sigma}\times\vec{\nabla}\Psi_\alpha(\vec{r}\,)$. As shown in section 2 of ref.[18] the Fourier transform of the expanded density-matrix eq.(1) with respect to both coordinates $\vec{a}$ and $\vec{r}$ defines in momentum space a "medium insertion":

$$\begin{aligned}\Gamma(\vec{p},\vec{q}\,) &= \int d^3r\, e^{-i\vec{q}\cdot\vec{r}}\,\Big\{\theta(k_f-|\vec{p}\,|) + \frac{\pi^2}{4k_f^4}\Big[k_f\,\delta'(k_f-|\vec{p}\,|) - 2\delta(k_f-|\vec{p}\,|)\Big] \\ &\quad \times\Big(\tau - \frac{3}{5}\rho k_f^2 - \frac{1}{4}\vec{\nabla}^2\rho\Big) - \frac{3\pi^2}{4k_f^4}\,\delta(k_f-|\vec{p}\,|)\,\vec{\sigma}\cdot(\vec{p}\times\vec{J})\Big\}\,, \end{aligned} \tag{2}$$

for inhomogeneous many-nucleon systems characterized by the time-reversal-even fields $\rho(\vec{r}\,)$, $\tau(\vec{r}\,)$ and $\vec{J}(\vec{r}\,)$. Note that the delta-function $\delta(k_f-|\vec{p}\,|)$ in eq.(2) gives weight to the momentum-dependent NN-interactions only in the vicinity of the local Fermi momentum, $|\vec{p}\,| = k_f(\vec{r}\,)$.

Up to second order in spatial gradients (i.e. deviations from homogeneity) the energy density functional relevant for $N = Z$ even-even nuclei reads:

$$\begin{aligned}\mathcal{E}[\rho,\tau,\vec{J}\,] &= \rho\,\bar{E}(\rho) + \Big[\tau - \frac{3}{5}\rho k_f^2\Big]\Big[\frac{1}{2M} - \frac{k_f^2}{4M^3} + F_\tau(\rho)\Big] \\ &\quad + (\vec{\nabla}\rho)^2\,F_\nabla(\rho) + \vec{\nabla}\rho\cdot\vec{J}\,F_{so}(\rho) + \vec{J}^{\,2}\,F_J(\rho)\,. \end{aligned} \tag{3}$$

Here, $\bar{E}(\rho)$ is the energy per particle of isospin-symmetric nuclear matter evaluated at the local nucleon density $\rho(\vec{r}\,)$. The strength function $F_\tau(\rho)$ introduces an effective (density-dependent) nucleon mass $M^*(\rho)$ and it is related to the single-particle potential $U(p,k_f)$ as follows:

$$F_\tau(\rho) = \frac{1}{2k_f}\frac{\partial U(p,k_f)}{\partial p}\Big|_{p=k_f} = -\frac{k_f}{3\pi^2}f_1(k_f)\,, \tag{4}$$

with $\rho = 2k_f^3/3\pi^2$. The second equality establishes the equivalent relation to the spin and isospin independent p-wave Landau parameter $f_1(k_f)$. The strength function $F_\nabla(\rho)$ of the $(\vec{\nabla}\rho)^2$ surface term has the decomposition [18]:

$$F_\nabla(\rho) = \frac{1}{4}\,\frac{\partial F_\tau(\rho)}{\partial\rho} + F_d(\rho)\,, \tag{5}$$

where $F_d(\rho)$ comprises all those contributions for which the $(\vec{\nabla}\rho)^2$-factor originated directly from the momentum dependence of the interactions in an expansion up to order $\vec{q}^{\,2}$. Note that only the (fixed) nuclear matter piece $\theta(k_f-|\vec{p}\,|)$ of the density-matrix expansion goes into the derivation of the strength function $F_d(\rho)$. The second to last term $\vec{\nabla}\rho\cdot\vec{J}\,F_{so}(\rho)$ in eq.(3) is responsible for the spin-orbit interaction in nuclei. The associated function $F_{so}(\rho)$ measures therefore the strength of the nuclear spin-orbit coupling.

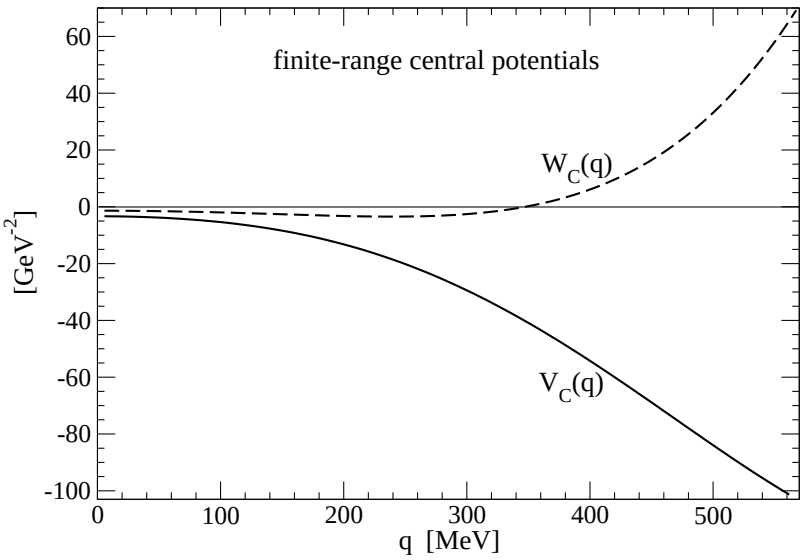

Figure 1: Finite-range isoscalar and isovector central potentials extracted from N^{3}LOW [22].

3 Two-body contributions

In this section we work out the two-body contributions to the various density-dependent strength functions which build up the nuclear energy density functional $\mathcal{E}[\rho,\tau,\vec{J}]$ written in eq.(3). Ideally, one would like to use for this task the universal low-momentum NN-potential $V_{\rm low-k}$ [12]. However, it is generally given in terms of (off-shell) partial wave matrix elements which makes its application to the density-matrix expansion rather cumbersome. An explicit representation of the momentum space NN-potential in terms of spin- and isospin-operators is much better suited for this purpose. For this reason we use (as a substitute for $V_{\rm low-k}$) the chiral NN-potential N^{3}LOW developed in refs.[21, 22] by lowering the cut-off scale to $\Lambda = 414\,$MeV. This value of Λ coincides with the resolution scale inherent to the universal low-momentum NN-potential $V_{\rm low-k}$. The finite-range part of the N^{3}LOW chiral NN-potential consists of one- and two-pion exchange pieces which can be summarized in the form:[2]

$$\begin{aligned} V_{NN}^{(\pi)} &= V_C(q) + \vec{\tau}_1\cdot\vec{\tau}_2\, W_C(q) + [V_S(q) + \vec{\tau}_1\cdot\vec{\tau}_2\, W_S(q)]\,\vec{\sigma}_1\cdot\vec{\sigma}_2 \\ &\quad + [V_T(q) + \vec{\tau}_1\cdot\vec{\tau}_2\, W_T(q)]\,\vec{\sigma}_1\cdot\vec{q}\,\vec{\sigma}_2\cdot\vec{q} \\ &\quad + [V_{SO}(q) + \vec{\tau}_1\cdot\vec{\tau}_2\, W_{SO}(q)]\, i(\vec{\sigma}_1+\vec{\sigma}_2)\cdot(\vec{q}\times\vec{p})\,, \end{aligned} \tag{6}$$

where $\vec{q}$ denotes the momentum transfer and $\vec{p}$ the center-of-mass momentum. As usual, $\vec{\sigma}_{1,2}$ and $\vec{\tau}_{1,2}$ are the spin- and isospin operators of the two nucleons. A special and simplifying feature of $V_{NN}^{(\pi)}$ is that all the occurring potentials $V_C(q),\ldots,W_{SO}(q)$ depend only on the momentum transfer q and that a quadratic spin-orbit component $\sim \vec{\sigma}_1\cdot(\vec{q}\times\vec{p})\,\vec{\sigma}_2\cdot(\vec{q}\times\vec{p})$ is absent. The relativistic $1/M^2$-correction to the 2π-exchange [24] which does (partially) not share this property is so small that it can be safely neglected. In order to specify our sign and normalization convention, we give also the explicit expression for the 1π-exchange, $W_T^{(1\pi)}(q) = -(g_A/2f_\pi)^2(m_\pi^2+q^2)^{-1}$, with the parameters $g_A = 1.3$, $f_\pi = 92.4\,$MeV and $m_\pi = 138\,$MeV.

The solid and dashed lines in Figs. 1,2,3,4 show the finite-range isoscalar and isovector potentials extracted from the chiral NN-interaction N^{3}LOW [22] in the central, spin-spin, tensor, and spin-orbit channel, respectively. In each figure the curves extend up to momentum transfers of $q = 570\,$MeV, corresponding to the region $q < 2k_f$ within which the interaction gets probed

[2]Note that we associate here the tensor interaction with the operator $\vec{\sigma}_1\cdot\vec{q}\,\vec{\sigma}_2\cdot\vec{q}$. This operator splits as $(q^2/3)[S_{12}(\hat{q}) + \vec{\sigma}_1\cdot\vec{\sigma}_2]$ into the genuine tensor operator $S_{12}(\hat{q})$ and a spin-spin piece.

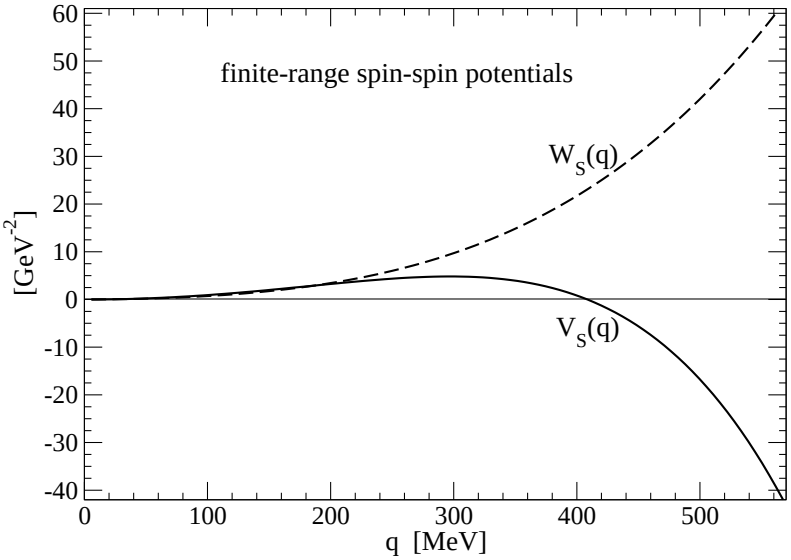

Figure 2: Finite-range isoscalar and isovector spin-spin potentials extracted from N^{3}LOW [22].

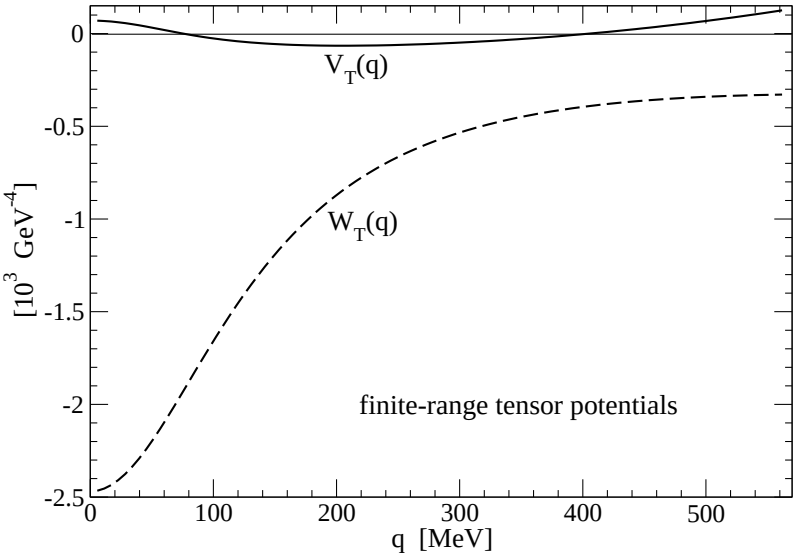

Figure 3: Finite-range isoscalar and isovector tensor potentials extracted from N^{3}LOW [22].

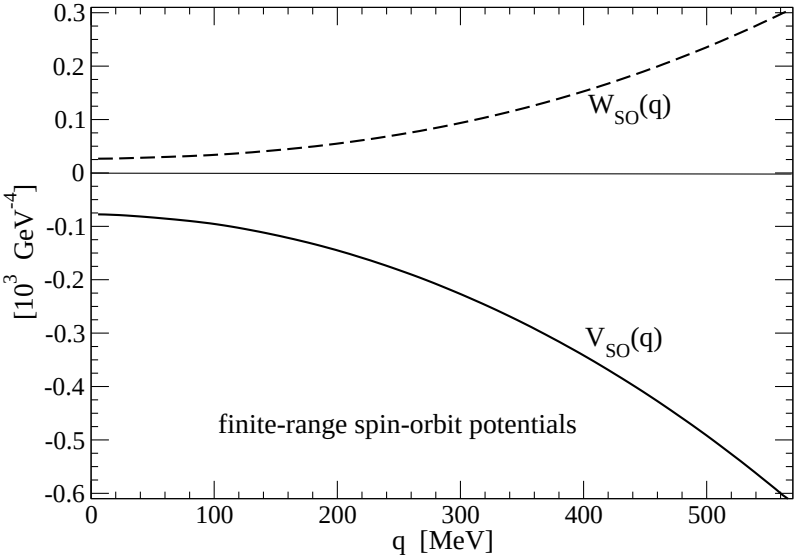

Figure 4: Finite-range isoscalar and isovector spin-orbit potentials extracted from N^{3}LOW [22].

for nuclear densities up to $\rho = 0.2\,\mathrm{fm}^{-3}$. One notices in Fig. 3 the large negative values of $W_T(q)$ (multiplied with $q^2/3$ in $V_{NN}^{(\pi)}$) which result at small momentum transfers from 1π-exchange.

In the (first-order) Hartree-Fock approximation the finite-range NN-potential $V_{NN}^{(\pi)}$ leads in combination with the density matrix-expansion (i.e. by employing the product of two medium insertions $\Gamma(\vec{p}_1,\vec{q})\,\Gamma(\vec{p}_2,-\vec{q})$), to the following two-body contributions to the energy density functional $\mathcal{E}[\rho,\tau,\vec{J}]$:

$$\begin{aligned}\bar{E}(\rho) &= \frac{\rho}{2}V_C(0) - \frac{3\rho}{2}\int_0^1 dx\, x^2(1-x)^2(2+x)\Big[V_C(q)+3W_C(q)\\ &\quad +3V_S(q)+9W_S(q)+q^2V_T(q)+3q^2W_T(q)\Big]\,, \end{aligned} \tag{7}$$

$$F_\tau(\rho) = \frac{k_f}{2\pi^2}\int_0^1 dx(x-2x^3)\Big[V_C(q)+3W_C(q)+3V_S(q)+9W_S(q)+q^2V_T(q)+3q^2W_T(q)\Big]\,, \tag{8}$$

$$F_d(\rho) = \frac{1}{4}V_C''(0) \simeq -27.1\,\mathrm{MeVfm}^5\,, \tag{9}$$

$$F_{so}(\rho) = \frac{1}{2}V_{SO}(0) + \int_0^1 dx\, x^3\Big[V_{SO}(2xk_f)+3W_{SO}(2xk_f)\Big]\,, \tag{10}$$

$$F_J(\rho) = \frac{3}{8k_f^2}\int_0^1 dx\Big\{(2x^3-x)\Big[V_C(q)+3W_C(q)-V_S(q)-3W_S(q)\Big]-x^3q^2\Big[V_T(q)+3W_T(q)\Big]\Big\}\,, \tag{11}$$

setting $q = 2xk_f$. The double-prime in eq.(9) denotes a second derivative and we have given the numerical value for $F_d(\rho)$ resulting from the negative curvature of isoscalar central potential $V_C(q)$ shown in Fig. 1. One can easily convince oneself that $F_J(\rho)$ as given in eq.(11) stays finite in the limit $k_f \to 0$. After expanding the integrand to linear order in q^2, the constant $V_C(0)+3W_C(0)$ integrates to zero.

In addition to the finite-range pieces written in eqs.(7-11) there are the two-body contributions from the zero-range contact potential of the chiral NN-interaction N^{3}LOW. The corresponding expression in momentum space includes constant, quadratic, and quartic terms in momenta and it can be found in section 2.2 of ref.[25]. The Hartree-Fock contributions from the NN-contact potential to the nuclear energy density functional $\mathcal{E}[\rho,\tau,\vec{J}]$ read:

$$\bar{E}(\rho) = \frac{3\rho}{8}(C_S-C_T) + \frac{3\rho k_f^2}{20}(C_2-C_1-3C_3-C_6) + \frac{9\rho k_f^4}{140}(D_2-4D_1-12D_5-4D_{11})\,, \tag{12}$$

$$F_\tau(\rho) = \frac{\rho}{4}(C_2-C_1-3C_3-C_6) + \frac{\rho k_f^2}{4}(D_2-4D_1-12D_5-4D_{11})\,, \tag{13}$$

$$F_d(\rho) = \frac{1}{32}(16C_1-C_2-3C_4-C_7) + \frac{k_f^2}{48}(9D_3+6D_4-9D_7-6D_8-3D_{12}-3D_{13}-2D_{15})\,, \tag{14}$$

$$F_{so}(\rho) = \frac{3}{8}C_5 + \frac{k_f^2}{6}(2D_9+D_{10})\,, \tag{15}$$

$$F_J(\rho) = \frac{1}{16}(2C_1-2C_3-2C_4-4C_6+C_7) + \frac{k_f^2}{32}(16D_1-16D_5-4D_6-24D_{11}+D_{14})\,. \tag{16}$$

The 24 low-energy constants $C_{S,T}$, C_j and D_j are determined (at the cut-off scale of $\Lambda = 414\,\mathrm{MeV}$) in fits to empirical NN-phase shifts and deuteron properties [22]. We have extracted their values from the pertinent NN-scattering code made available to us by R. Machleidt. The values of the low-energy constants for the pure contact terms are: $C_S = -117.5$, $C_T = 2.937$ (in units GeV^{-2}), those of the terms quadratic in momenta are: $C_1 = 475.8$, $C_2 = 1034.1$, $C_3 = -29.04$, $C_4 = -524.4$, $C_5 = 717.4$, $C_6 = -42.70$, $C_7 = -1753.6$ (in units GeV^{-4}), and those of the terms quartic in momenta are: $D_1 = 0.612$, $D_2 = 25.61$, $D_3 = 19.68$, $D_4 = -19.49$,

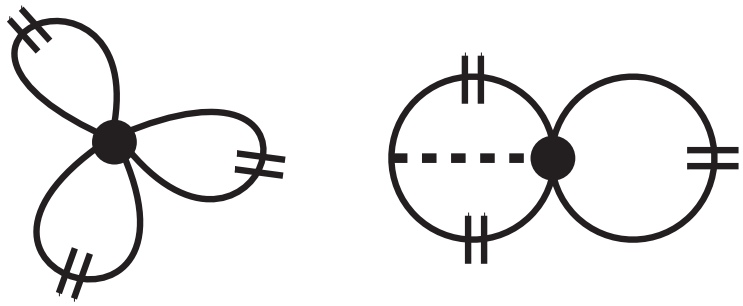

Figure 5: Three-body diagrams related to the contact (c_E) and 1π-exchange (c_D) component of the chiral three-nucleon interaction. The short double-line symbolizes the medium insertion $\Gamma(\vec{p},\vec{q}\,)$ for inhomogeneous nuclear matter.

$D_5 = 1.287$, $D_6 = 19.02$, $D_7 = 6.565$, $D_8 = -5.429$, $D_9 = 4.226$, $D_{10} = -16.02$, $D_{11} = -1.243$, $D_{12} = -0.976$, $D_{13} = -0.998$, $D_{14} = -7.995$, $D_{15} = -0.491$ (in units $10^3\,\mathrm{GeV}^{-6}$). Let us mention that the contributions proportional to $C_{S,T}$ and C_j in eqs.(12-16) have also been worked out in appendix B of ref.[19] and we find agreement with their results. The terms proportional to D_j as well as the master formulas eqs.(7-11) for the finite-range contributions are new. Note that we do not include an additional regulator function [22] since the NN-interactions are probed only at small momenta $|\vec{p}_{1,2}| \leq k_f \leq 285\,\mathrm{MeV}$.

4 Three-body contributions

In this section we work out the three-body contributions to the nuclear energy density functional $\mathcal{E}[\rho,\tau,\vec{J}]$. We employ the leading order chiral three-nucleon interaction [23] which consists of a contact piece (with parameter c_E), a 1π-exchange component (with parameter c_D) and a 2π-exchange component (with parameters c_1, c_3 and c_4). In order to treat the three-body correlations in inhomogeneous nuclear many-body systems we follow ref.[18] and assume that the relevant product of density-matrices can be represented in momentum space in a factorized form by $\Gamma(\vec{p}_1,\vec{q}_1)\,\Gamma(\vec{p}_2,\vec{q}_2)\,\Gamma(\vec{p}_3,-\vec{q}_1-\vec{q}_2)$. Such a factorization ansatz respects by construction the correct nuclear matter limit, but it involves approximations in comparison to more sophisticated treatments outlined in section 4 of ref.[9]. Actually, our approach is similar to the method DME-I introduced in ref.[9].

4.1 c_E-term

We start with the three-body contributions from the contact interaction as represented by the left diagram in Fig. 5. With three (inhomogeneous) medium insertions one finds the following contribution to the energy per particle:

$$\bar{E}(\rho) = -\frac{c_E k_f^6}{12\pi^4 f_\pi^4 \Lambda_\chi}\,, \tag{17}$$

which is quadratic in the density $\rho = 2k_f^3/3\pi^2$. Obviously, the contributions to the other strength functions $F_{\tau,d,so,J}(\rho)$ vanish due to the momentum-independence of the contact interaction. For the choice of scale $\Lambda_\chi = 700\,\mathrm{MeV}$ the value $c_E = -0.625$ has been determined in calculations of few-nucleon systems [13] (employing in addition $V_{\mathrm{low-k}}$ for the two-body interaction).

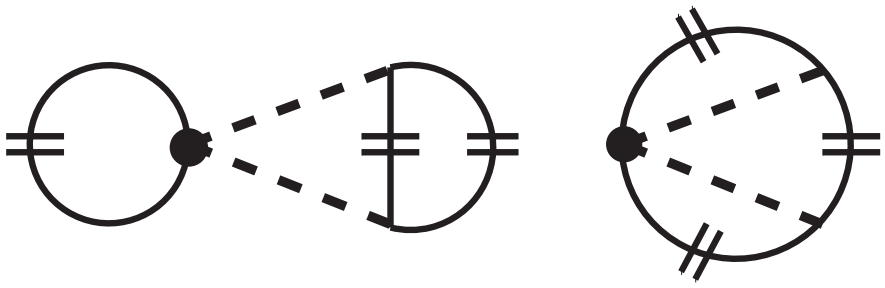

Figure 6: Three-body Hartree and Fock diagrams related to the chiral 2π-exchange three-nucleon interaction.

4.2 c_D-term

Next, we consider the three-body contributions from the 1π-exchange component of the chiral 3N-interaction as represented by the right diagram in Fig. 5. Putting in three (inhomogeneous) medium insertions one finds the following analytical expressions:

$$\bar{E}(\rho) = \frac{g_A c_D m_\pi^6}{(2\pi f_\pi)^4 \Lambda_\chi} \Big\{ \frac{u^6}{3} - \frac{3u^4}{4} + \frac{u^2}{8} + u^3 \arctan 2u - \frac{1+12u^2}{32} \ln(1+4u^2) \Big\} , \tag{18}$$

$$F_\tau(\rho) = \frac{2 g_A c_D m_\pi^4}{(4\pi f_\pi)^4 \Lambda_\chi} \Big\{ (1+2u^2) \ln(1+4u^2) - 4u^2 \Big\} , \tag{19}$$

$$F_d(\rho) = \frac{g_A c_D m_\pi}{(4 f_\pi)^4 \pi^2 \Lambda_\chi} \Big\{ \frac{1}{2u} \ln(1+4u^2) - \frac{2u}{1+4u^2} \Big\} , \tag{20}$$

$$F_J(\rho) = \frac{3 g_A c_D m_\pi}{(4 f_\pi)^4 \pi^2 \Lambda_\chi} \Big\{ 2u - \frac{1}{u} + \frac{1}{4u^3} \ln(1+4u^2) \Big\} , \tag{21}$$

with the abbreviation $u = k_f/m_\pi$. For the parameter c_D we take the value $c_D = -2.06$ from ref.[13]. Note that there is no contribution to the spin-orbit coupling strength $F_{so}(\rho)$.

4.3 Hartree diagram proportional to $c_{1,3}$

We continue with the three-body contributions from the 2π-exchange Hartree diagram shown in the left part of Fig. 6. Again with three (inhomogeneous) medium insertions one derives the following analytical results:

$$\begin{aligned} \bar{E}(\rho) &= \frac{g_A^2 m_\pi^6}{(2\pi f_\pi)^4} \Big\{ (12c_1 - 10c_3) u^3 \arctan 2u - \frac{4}{3} c_3 u^6 + 6(c_3 - c_1) u^4 \\ &\quad + (3c_1 - 2c_3) u^2 + \Big[\frac{1}{4}(2c_3 - 3c_1) + \frac{3u^2}{2}(3c_3 - 4c_1) \Big] \ln(1+4u^2) \Big\} , \end{aligned} \tag{22}$$

$$\begin{aligned} F_\tau(\rho) &= \frac{g_A^2 m_\pi^4}{(2\pi f_\pi)^4} \Big\{ (5c_3 - 6c_1) u^2 + \frac{(c_3 - 2c_1) u^2}{1+4u^2} \\ &\quad + \Big[2c_1 - \frac{3}{2} c_3 + 2(c_1 - c_3) u^2 \Big] \ln(1+4u^2) \Big\} , \end{aligned} \tag{23}$$

$$\begin{aligned} F_d(\rho) &= \frac{g_A^2 m_\pi}{(8\pi)^2 f_\pi^4} \Big\{ (10c_1 - 23c_3) \arctan 2u + 16 c_3 u \\ &\quad + \frac{7c_3 - 5c_1}{u} \ln(1+4u^2) + \frac{6c_3 u + 16(2c_3 - c_1) u^3}{3(1+4u^2)^2} \Big\} , \end{aligned} \tag{24}$$

$$F_{so}(\rho) = \frac{3g_A^2 m_\pi}{(8\pi)^2 f_\pi^4}\Big\{\frac{2}{u}(4c_1-3c_3) - 4c_3 u + \Big[\frac{4}{u}(c_3-c_1) + \frac{3c_3-4c_1}{2u^3}\Big]\ln(1+4u^2)\Big\}, \qquad (25)$$

$$F_J(\rho) = \frac{3g_A^2 m_\pi}{(8\pi)^2 f_\pi^4}\Big\{\frac{3c_3-4c_1}{u} - 2c_3 u + \frac{4u(2c_1-c_3)}{1+4u^2} + \frac{4c_1-3c_3}{4u^3}\ln(1+4u^2)\Big\}, \qquad (26)$$

which depend only on the two isoscalar coupling constants c_1 and c_3 with values $c_1 = -0.76\,\mathrm{GeV}^{-1}$ and $c_3 = -4.78\,\mathrm{GeV}^{-1}$ [23]. Note that the expression for $F_{so}(\rho)$ in eq.(25) gives the dominant part of the three-body spin-orbit coupling strength suggested originally by Fujita and Miyazawa [26]. Their proposed mechanism is based on the excitation of a $\Delta(1232)$-resonance. In the present approach the two-step process $\pi N \to \Delta \to \pi N$ is replaced by an equivalent $\pi\pi NN$ contact vertex proportional to c_3.

4.4 Fock diagram proportional to $c_{1,3,4}$

Finally, there are the three-body contributions from the 2π-exchange Fock diagram shown in the right part of Fig. 6. With one single closed nucleon ring this diagram generates (for isospin-symmetric nuclear matter) also non-vanishing contributions from the isovector $\pi\pi NN$ contact vertex proportional to c_4. We take consistently the value $c_4 = 3.96\,\mathrm{GeV}^{-1}$ used in few-body calculations by ref.[23]. In the case of the three-body Fock diagram not all of the occurring integrals over the three Fermi spheres can be solved analytically. Collecting all the emerging pieces, we find the following results for the Fock contributions to the nuclear energy density functional $\mathcal{E}[\rho,\tau,\vec{J}]$:

$$\begin{aligned}\bar{E}(\rho) &= \frac{3g_A^2 m_\pi^6}{(4\pi f_\pi)^4 u^3}\int_0^u dx\Big\{\Big(\frac{c_3}{2}-c_4\Big)G_S^2 + (c_3+c_4)G_T^2 + 3c_1 \\ &\quad \times\Big[u(1+u^2+x^2) - \Big(1+(u+x)^2\Big)\Big(1+(u-x)^2\Big)L\Big]^2\Big\}, \qquad (27)\end{aligned}$$

$$\begin{aligned}F_\tau(\rho) &= \frac{g_A^2 m_\pi^4}{(4\pi f_\pi)^4}\Big\{\frac{2}{u^3}(2c_4-c_3)\Big[4u^2-(1+2u^2)\ln(1+4u^2)\Big]\arctan 2u \\ &\quad +\frac{1+2u^2}{64u^8}\Big[48(c_4-c_3-2c_1)u^4 - 8(3c_1+2c_3+2c_4)u^2 - 3(c_3+c_4)\Big] \\ &\quad \times\ln^2(1+4u^2) + \Big[\frac{4}{3}(c_3-5c_4)u^2 + 6c_1 - \frac{7}{3}c_3 + \frac{17}{3}c_4 + \frac{3}{8u^6}(c_3+c_4) \\ &\quad +\frac{24c_1+5(c_3+c_4)}{2u^2} + \frac{3c_1+2(c_3+c_4)}{u^4}\Big]\ln(1+4u^2) + \frac{8}{3}(c_3+c_4)u^4 \\ &\quad +\frac{2u^2-3}{3}(17c_4-7c_3) - 12c_1 - \frac{12c_1+5(c_3+c_4)}{2u^2} - \frac{3}{4u^4}(c_3+c_4) \\ &\quad +\frac{1}{u^3}\int_0^u dx\Big\{12c_1\Big[u(1+u^2+x^2) - \Big(1+(u+x)^2\Big)\Big(1+(u-x)^2\Big)L\Big] \\ &\quad \times\Big[(1-u^2-x^2)L + u - \frac{u}{1+(u+x)^2} - \frac{u}{1+(u-x)^2}\Big] \\ &\quad +(2c_4-c_3)G_S\Big[\frac{2u(u+x)}{1+(u+x)^2} + \frac{2u(x-u)}{1+(u-x)^2} - 4xL\Big] \\ &\quad -(c_3+c_4)G_T\Big[\frac{3u}{x}(3u^2-1) - 3ux + \frac{4u(u+x)}{1+(u+x)^2} + \frac{4u(x-u)}{1+(u-x)^2} \\ &\quad +\frac{L}{x}(3x^4+6u^2x^2-2x^2-9u^4-6u^2+3)\Big]\Big\}\Big\}, \qquad (28)\end{aligned}$$

$$
\begin{aligned}
F_d(\rho) &= \frac{g_A^2 m_\pi}{\pi^2(4f_\pi)^4}\Big\{c_1\Big[\frac{16u}{1+4u^2}-\frac{6}{u}+\Big(\frac{3}{u^3}-\frac{4}{u}+\frac{16u}{1+4u^2}\Big)\ln(1+4u^2)\\
&\quad -\frac{3}{8u^5}\ln^2(1+4u^2)\Big]+(c_3+c_4)\Big[\frac{3}{u}-\frac{3}{2u^3}-\frac{12u}{1+4u^2}\\
&\quad +\Big(\frac{3}{4u^5}+\frac{5}{2u}-\frac{8u}{1+4u^2}\Big)\ln(1+4u^2)-\frac{3+6u^2+8u^4}{32u^7}\ln^2(1+4u^2)\Big]\\
&\quad +c_4\Big[\frac{8u}{1+4u^2}+\Big(\frac{8u}{1+4u^2}-\frac{4}{u}\Big)\ln(1+4u^2)+\frac{1}{2u^3}\ln^2(1+4u^2)\Big]\Big\}, \qquad (29)
\end{aligned}
$$

$$
\begin{aligned}
F_{so}(\rho) &= \frac{g_A^2 m_\pi}{\pi^2(4f_\pi u)^4}\Big\{3c_1\Big[2u-2u^3+\frac{3}{2u}-\frac{3+10u^2}{4u^3}\ln(1+4u^2)\\
&\quad +\frac{3+16u^2+16u^4}{32u^5}\ln^2(1+4u^2)\Big]+(c_3+c_4)\Big[u^3-\frac{16u^5}{3}+\frac{7u}{4}\\
&\quad +\frac{3}{u}+\frac{15}{16u^3}+\Big(2u^3-\frac{3u}{2}-\frac{13}{4u}-\frac{39}{16u^3}-\frac{15}{32u^5}\Big)\ln(1+4u^2)\\
&\quad +\frac{3}{256u^7}(64u^6+80u^4+36u^2+5)\ln^2(1+4u^2)\Big]\Big\}, \qquad (30)
\end{aligned}
$$

$$
\begin{aligned}
F_J(\rho) &= \frac{9g_A^2 c_1 m_\pi}{\pi^2(4f_\pi u)^4}\Big\{\frac{10u^3}{3}+\frac{11u}{8}-\frac{1}{2u}+\frac{8+9u^2-76u^4}{32u^3}\ln(1+4u^2)\\
&\quad -\frac{1}{2}\arctan 2u-\frac{1+4u^2}{32u^5}\ln^2(1+4u^2)+\int_0^u dx\Big\{\frac{L^2}{u^2}\Big[\frac{3}{4x^2}(1+u^2)^4\\
&\quad +(1+u^2)(1-u^4)+\frac{11x^6}{4}+5(1-u^2)x^4+\frac{x^2}{2}(5u^4-14u^2+5)\Big]\\
&\quad +\frac{L}{2u}\Big[3u^4+2u^2-1-\frac{3}{x^2}(1+u^2)^3\Big]+\frac{3}{4x^2}(1+u^2)^2\Big\}\Big\}\\
&+ \frac{3g_A^2 c_3 m_\pi}{\pi^2(8f_\pi u)^4}\Big\{\Big[7+65u^2-34u^4+8u^{-2}\ln(1+4u^2)\Big]\arctan 2u\\
&\quad +\frac{832u^5}{5}-\frac{1415u^3}{12}+\frac{91u}{4}-\frac{4}{u}-\frac{3}{u^3}-\frac{3+16u^2+48u^4}{16u^7}\\
&\quad \times\ln^2(1+4u^2)+\Big(\frac{3}{2u^5}+\frac{5}{u^3}-\frac{103}{16u}+\frac{221u}{48}-\frac{15u^3}{4}\Big)\ln(1+4u^2)\\
&\quad +\int_0^u dx\Big\{\frac{3L^2}{2u^2}\Big[\frac{5}{x^4}(1+u^2)^6+\frac{6}{x^2}(1+u^2)^4(1-3u^2)+(1+u^2)^2\\
&\quad \times(23-18u^2+39u^4)+4x^2(9+23u^2-5u^4-19u^6)+17x^8\\
&\quad +x^4(19-26u^2+99u^4)+22x^6(1-3u^2)\Big]+\frac{L}{u}\Big[-\frac{15}{x^4}(1+u^2)^5\\
&\quad +\frac{1}{x^2}(1+u^2)^3(49u^2-3)-6(17u^6+13u^4+7u^2+11)\Big]\\
&\quad +\frac{15}{2x^4}(1+u^2)^4-\frac{2}{x^2}(1+u^2)^2(3+11u^2)\Big\}\Big\}\\
&+ \frac{3g_A^2 c_4 m_\pi}{\pi^2(8f_\pi u)^4}\Big\{\Big[79-95u^2-10u^4-16u^{-2}\ln(1+4u^2)\Big]\arctan 2u\\
&\quad -\frac{512u^5}{15}+\frac{2185u^3}{12}-\frac{181u}{4}-\frac{4}{u}-\frac{3}{u^3}+\frac{48u^4-16u^2-3}{16u^7}
\end{aligned}
$$

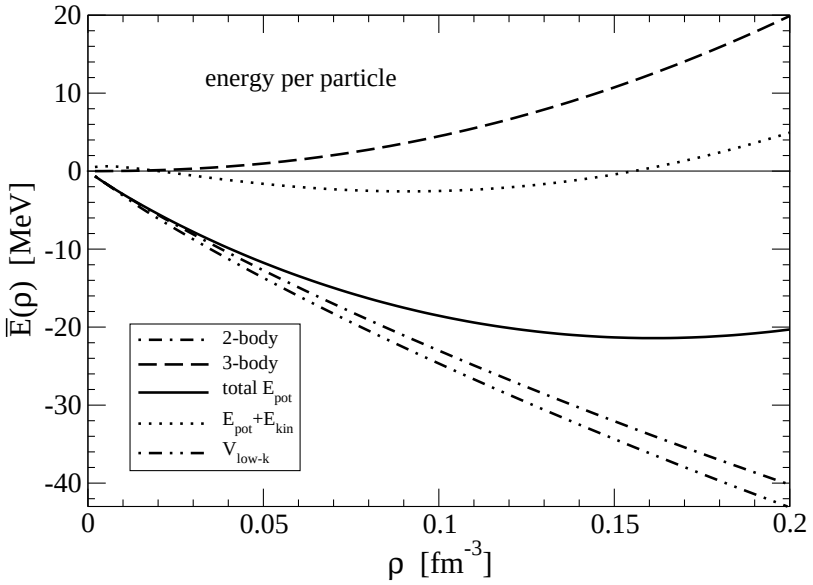

Figure 7: Contributions to the energy per particle $\bar{E}(\rho)$ of isospin-symmetric nuclear matter.

$$
\begin{aligned}
&\times \ln^2(1+4u^2) + \left(\frac{3}{2u^5} + \frac{5}{u^3} - \frac{119}{16u} + \frac{173u}{48} + \frac{9u^3}{4}\right)\ln(1+4u^2) \\
&+ \int_0^u dx \left\{ \frac{3L^2}{2u^2}\Big[\frac{5}{x^4}(1+u^2)^6 + \frac{6}{x^2}(1+u^2)^4(1-3u^2) + (1+u^2)^2 \right. \\
&\times(7+14u^2+23u^4) + 4x^2(9+7u^2-5u^4-3u^6) + x^8 \\
&+x^4(51-26u^2+3u^4) + x^6(22-2u^2)\Big] + \frac{L}{u}\Big[-\frac{15}{x^4}(1+u^2)^5 \\
&+\frac{1}{x^2}(1+u^2)^3(49u^2-3) - 18(1+3u^2)(1+u^2)^2\Big] \\
&\left. +\frac{15}{2x^4}(1+u^2)^4 - \frac{2}{x^2}(1+u^2)^2(3+11u^2)\right\}\Bigg\}\,. \qquad (31)
\end{aligned}
$$

Here we have introduced the auxiliary functions:

$$
\begin{aligned}
G_S(x,u) &= \frac{4ux}{3}(2u^2-3) + 4x\Big[\arctan(u+x) + \arctan(u-x)\Big] \\
&\quad +(x^2-u^2-1)\ln\frac{1+(u+x)^2}{1+(u-x)^2}\,, \qquad (32) \\
G_T(x,u) &= \frac{ux}{6}(8u^2+3x^2) - \frac{u}{2x}(1+u^2)^2 \\
&\quad +\frac{1}{8}\Big[\frac{(1+u^2)^3}{x^2} - x^4 + (1-3u^2)(1+u^2-x^2)\Big]\ln\frac{1+(u+x)^2}{1+(u-x)^2}\,, \qquad (33) \\
L(x,u) &= \frac{1}{4x}\ln\frac{1+(u+x)^2}{1+(u-x)^2}\,, \qquad (34)
\end{aligned}
$$

where $u = k_f/m_\pi$. A good check of all formulas collected in this section is provided by their Taylor expansion in k_f. Despite the superficial first appearance to the contrary, one can verify that the leading term in the k_f-expansion is k_f^3. In several cases it is even a higher power of k_f.

5 Results and discussion

In this section we present and discuss our numerical results obtained by summing the series of two- and three-body contributions given in sections 3 and 4. The physical input parameters

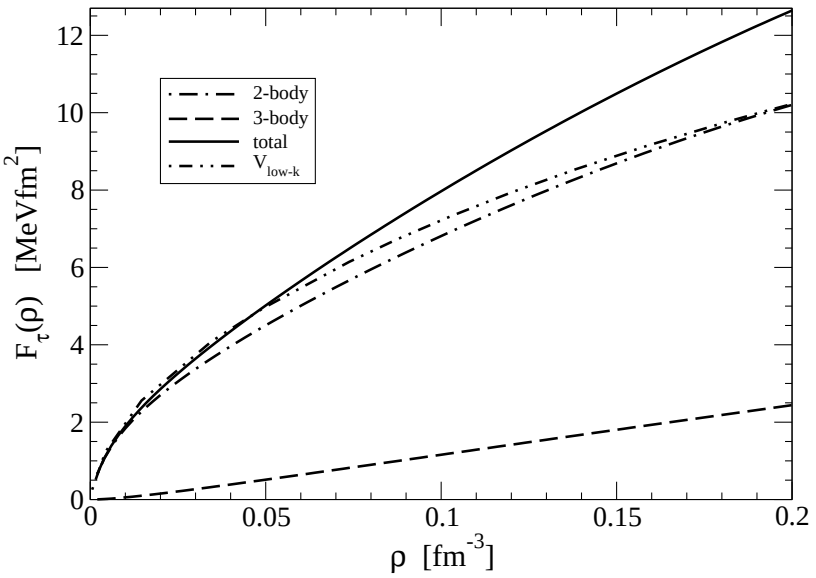

Figure 8: Contributions to the strength function $F_\tau(\rho)$ versus the nuclear density ρ.

are: $g_A = 1.3$ (nucleon axial vector coupling constant), $f_\pi = 92.4\,\mathrm{MeV}$ (pion decay constant) and $m_\pi = 138\,\mathrm{MeV}$ (average pion mass). The parameters $C_{S,T}$, C_j and D_j corresponding to the 24 contact terms in the chiral NN-potential N^{3}LOW [22] have already been listed at the end of section 3. For the sake of completeness we quote again the parameters pertinent to the chiral three-nucleon interaction: $c_E = -0.625$, $c_D = -2.06$, $\Lambda_\chi = 700\,\mathrm{MeV}$, $c_1 = -0.76\,\mathrm{GeV}^{-1}$, $c_3 = -4.78\,\mathrm{GeV}^{-1}$ and $c_4 = 3.96\,\mathrm{GeV}^{-1}$, taken from refs.[13, 23].

Fig.7 shows the contributions to the energy per particle $\bar{E}(\rho)$ of isospin-symmetric nuclear matter for densities up to $\rho = 0.2\,\mathrm{fm}^{-3}$. The dash-dotted line gives the (attractive) two-body contributions and the dashed line the (repulsive) three-body contributions. For comparison we have also included the Hartree-Fock contribution to the energy per particle $\bar{E}(\rho)$ as obtained from the universal low-momentum NN-potential $V_{\mathrm{low-k}}$ [11, 12, 13] by summing and integrating its diagonal (on-shell) partial-wave matrix elements. One observes that our treatment of the NN-interaction via the chiral potential N^{3}LOW reproduces these results fairly accurately. The sum of the two- and three-body contributions (full line in Fig. 7) shows a first tendency for saturation of nuclear matter. However, after inclusion of the kinetic energy $\bar{E}_{\mathrm{kin}}(\rho) = 3k_f^2/10M - 3k_f^4/56M^3$ the resulting minimum is still much too shallow. This observation (at the Hartree-Fock level) is consistent with refs.[13, 14]. An improved description of the nuclear matter equation of state $\bar{E}(\rho)$ can be achieved when treating the two-body interaction at least to second order.

Fig. 8 shows the contributions to the strength function $F_\tau(\rho)$. For the two-body part the results derived with $V_{\mathrm{low-k}}$ and the chiral N^{3}LOW potential lie closely together. The three-body part (shown by the dashed line in Fig. 8) comes out relatively small. At $\rho_0 = 0.16\,\mathrm{fm}^{-3}$ it adds a correction of about 20%. The expression multiplying the kinetic energy density $\tau(\vec{r}\,)$ in the nuclear energy density functional eq.(3) has the meaning of a reciprocal density-dependent effective nucleon mass:

$$M^*(\rho) = M\left[1 - \frac{k_f^2}{2M^2} + 2M\,F_\tau(\rho)\right]^{-1}. \tag{35}$$

It is identical to the so-called "Landau"-mass introduced in Fermi-liquid theory, since it derives in the same way from the slope of the single-particle potential $U(p, k_f)$ at the Fermi surface $p = k_f$. The (small) correction term $-k_f^2/2M^2$ accounts for the relativistic increase of mass. Fig. 9 shows the ratio of effective to free nucleon mass $M^*(\rho)/M$ as a function of the nuclear density ρ. One observes a reduced effective nucleon mass which reaches the value $M^*(\rho_0) \simeq 0.67M$ at nuclear matter saturation density $\rho_0 = 0.16\,\mathrm{fm}^{-3}$. This is compatible with the range

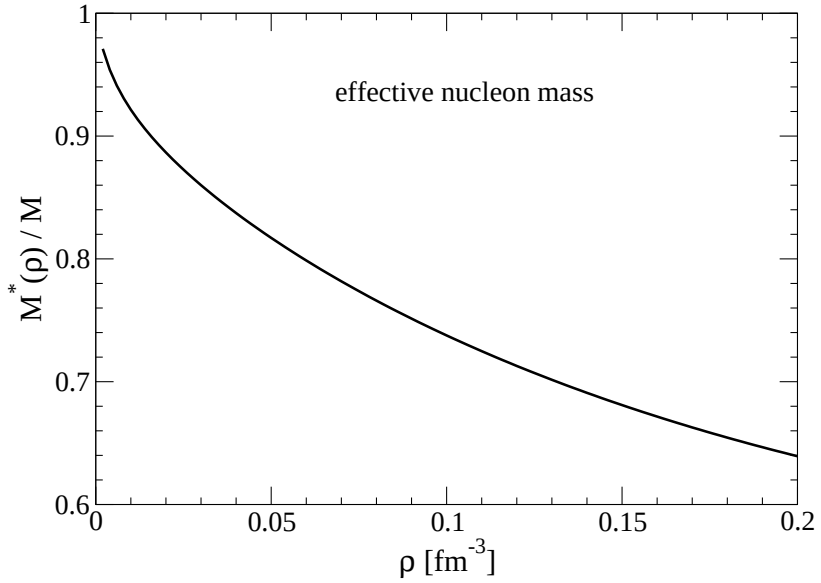

Figure 9: Effective nucleon mass $M^*(\rho)$ divided by free nucleon mass M as function of ρ.

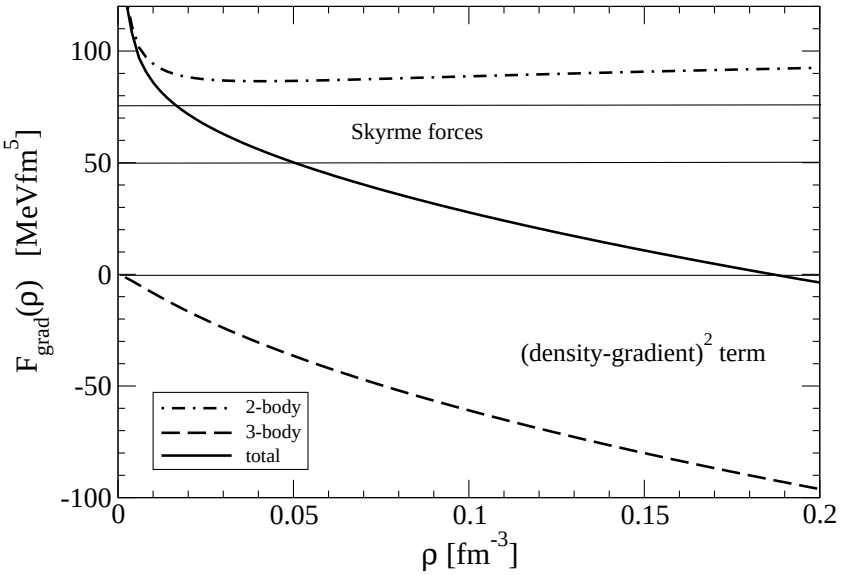

Figure 10: The strength function $F_\nabla(\rho)$ of the surface term $(\vec{\nabla}\rho)^2$ versus the nuclear density ρ.

$0.7 < M^*(\rho_0)/M < 1$ spanned by phenomenological Skyrme forces [3, 4]. On the other hand it has been found recently in ref.[27] that second-order corrections from $V_{\mathrm{low-k}}$ enhance the effective nucleon mass substantially.

Next, we show in Fig. 10 the strength function $F_\nabla(\rho)$ of the $(\vec{\nabla}\rho)^2$ surface-term. The pronounced increase of the two-body contribution (dash-dotted line) at very low densities is caused by the 1π-exchange and has also been observed in other calculations [18, 19]. The sizeable three-body contribution (dashed line) adds negatively to these initial values such that the total result for $F_\nabla(\rho)$ (shown by the full line in Fig. 10) decreases with increasing density ρ. For comparison we have also included the band (of constant $F_\nabla(\rho)$-values) spanned by phenomenological Skyrme forces [3, 4]. Taking this as a benchmark one sees that our Hartree-Fock result is somewhat too small at densities around $\rho_0/2 = 0.08\,\mathrm{fm}^{-3}$, where the surface energy in nuclei gains most of its weight. The calculation of the iterated 1π-exchange in ref.[18] suggests that a treatment of the low-momentum two-body interaction to second order will further increase the values of $F_\nabla(\rho)$.

Of particular interest is the strength function $F_{so}(\rho)$ of the spin-orbit coupling term $\vec{\nabla}\rho \cdot \vec{J}$.

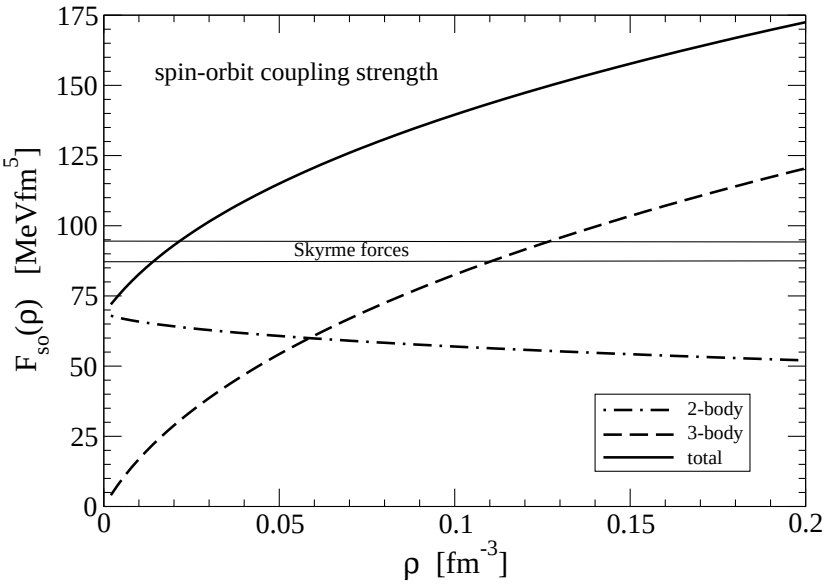

Figure 11: Strength function $F_{so}(\rho)$ of the spin-orbit coupling term $\vec{\nabla}\rho \cdot \vec{J}$ versus ρ.

The two- and three-body contributions together with their total sum are shown in Fig. 11. The two-body part is dominated by the low-energy constant $3C_5/8$ as indicated also by the weak variation of the dash-dotted line with density ρ. The induced (density-dependent) three-body spin-orbit forces add sizeably to this initial value. The major contribution is provided by the Hartree term in eq.(23) proportional to $c_3 = -4.78\,\mathrm{GeV}^{-1}$. With this given value of c_3 it is considerably larger than the $\Delta(1232)$-excitation mechanism proposed by Fujita and Miyazawa [26] which corresponds to $c_3^{(\Delta)} = -g_A^2/2\Delta \simeq -2.9\,\mathrm{GeV}^{-1}$ (with $\Delta = 293\,\mathrm{MeV}$ the delta-nucleon mass splitting). At densities around $\rho_0/2 = 0.08\,\mathrm{fm}^{-3}$ where the spin-orbit interaction in nuclei receives most of its weight, our total Hartree-Fock result overshoots the empirical spin-orbit coupling strength $F_{so}^{(\mathrm{emp})}(\rho) \simeq 90\,\mathrm{MeVfm}^5$ [3, 4] by about 50%. This requires a compensating effect, and indeed it has been found in ref.[18] that the second-order 1π-exchange tensor force generates a spin-orbit coupling of the "wrong-sign". Taking the value $F_{so}^{(1\pi-\mathrm{it})}(\rho_0/2) \simeq -35\,\mathrm{MeVfm}^5$ (see Fig. 5 in ref.[18]) as indicative one can expect that the second-order effects from the low-momentum two-nucleon tensor potential will reduce the strength of the spin-orbit coupling $F_{so}(\rho)$ to the correct amount.

Finally, we show in Fig. 12 the strength function $F_J(\rho)$ of the squared spin-orbit density $\vec{J}^2$ in the nuclear energy density functional $\mathcal{E}[\rho, \tau, \vec{J}]$. In contrast to all previous quantities, $F_J(\rho)$ receives only a very small three-body contribution. On the other hand the two-body contribution is strongly density-dependent and it reaches quite large values at low densities. This prominent feature of $F_J(\rho)$ has also been observed in previous calculations [18, 19]. Actually, the strong density dependence of $F_J(\rho)$ originates from the dominant 1π-exchange contribution which we reproduce separately in Fig. 12 by the upper dash-dotted line (for an explicit formula for $F_J^{(1\pi)}(\rho)$, see eq.(11) in ref.[18]). At this point it should be kept in mind that the $\vec{J}^2$-term in the nuclear energy density functional represents the non-local Fock contributions from tensor forces etc. An outstanding 1π-exchange contribution to the strength function $F_J(\rho)$ is therefore not surprising.

6 Summary and outlook

In this work we have used the (improved) density-matrix expansion of ref.[17] to calculate the nuclear energy density functional from chiral two- and three-nucleon interactions. We have

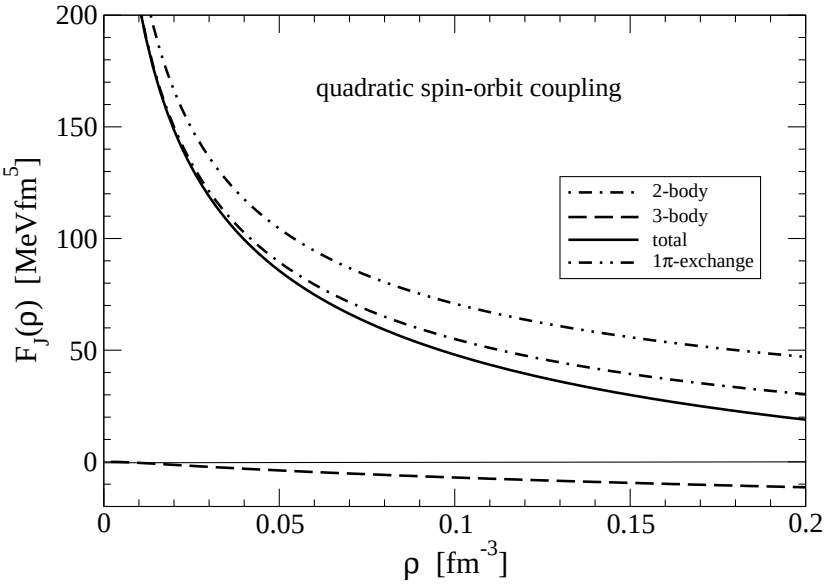

Figure 12: The strength function $F_J(\rho)$ multiplying the squared spin-orbit density $\vec{J}^2$ versus ρ.

employed the low-momentum NN-potential N^{3}LOW [22] which is composed of long-range multi-pion exchanges and a set of short-distance contact terms. The coefficients of the latter have been determined in fits to empirical NN-phase shifts. The leading order chiral three-nucleon interaction has been taken with its parameters c_E, c_D and $c_{1,3,4}$ fixed in calculations of nuclear few-body systems [13, 23]. With this input the nuclear energy density functional $\mathcal{E}[\rho, \tau, \vec{J}]$ has been derived to first order in many-body perturbation theory, i.e. in the Hartree-Fock approximation. For the effective nucleon mass $M^*(\rho)$ and the strength functions $F_\nabla(\rho)$ and $F_{so}(\rho)$ of the surface and spin-orbit terms we have found (in the relevant density range) reasonable agreement with results of phenomenological Skyrme forces. However, as indicated in particular by the nuclear matter equation of state $\bar{E}(\rho)$, an improved description of the energy density functional requires at least the treatment of the two-nucleon interaction to second order in many-body perturbation theory. It is furthermore expected that tensor forces at second-order generate an additional "wrong-sign" spin-orbit coupling [18] which compensates part of the strong three-body contribution to $F_{so}(\rho)$.

Such a consistent second-order calculation of the nuclear energy density functional represents a challenge, since a satisfactory generalization of the density-matrix expansion [19] to that situation has not yet been formulated. At second order one must properly account for the presence of energy denominators which induce further spatial and temporal non-localities and possibly even an orbital dependence of the resulting energy density functional. In a first simplified approach one could follow ref.[18] and approximate the energy denominators by the kinetic energies of free (on-shell) nucleons, eventually improved by the inclusion of an effective nucleon mass $M^*(\rho)$. In order to keep the second-order calculation manageable and in order to see leading effects, one would also restrict the low-momentum two-nucleon interaction to some dominant components, such as one-pion exchange with a suitable regularization of its strong tensor force at short distances. Studies along this line are underway.

Acknowledgement

We thank R. Machleidt for providing us the code for elastic NN-scattering with the chiral potential N^{3}LOW.

References

[1] M. Bender, P.H. Heenen and P.G. Reinhard, *Rev. Mod. Phys.* **75** (2003) 121.

[2] J.R. Stone and P.G. Reinhard, *Prog. Part. Nucl. Phys.* **58** (2007) 587.

[3] E. Chabanat et al., *Nucl. Phys.* **A627** (1997) 710; **A635** (1998) 231; and refs. therein.

[4] N. Chamel, S. Goriely and J.M. Pearson, *Nucl. Phys.* **A812** (2008) 72.

[5] B.D. Serot and J.D. Walecka, *Int. J. Mod. Phys.* **E6** (1997) 515.

[6] T. Niksic, D. Vretenar and P. Ring, nucl-th/1102.4193; to be published in *Prog. Part. Nucl. Phys.* (2011).

[7] T. Lesinski, T. Duguet, K. Bennaceur and J. Meyer, *Eur. Phys. J.* **A40** (2009) 121.

[8] J.E. Drut, R.J. Furnstahl and L. Platter, *Prog. Part. Nucl. Phys.* **64** (2010) 120; nucl-th/0906.1463.

[9] S.K. Bogner, R.J. Furnstahl and L. Platter, *Eur. Phys. J.* **A39** (2009) 219.

[10] J.E. Drut and L. Platter, nucl-th/1104.4357.

[11] S.K. Bogner, R.J. Furnstahl and A. Schwenk, *Prog. Part. Nucl. Phys.* **65** (2010) 94.

[12] S.K. Bogner, T.T.S. Kuo and A. Schwenk, *Phys. Reports* **386** (2003) 1.

[13] S.K. Bogner, R.J. Furnstahl, A. Nogga and A. Schwenk, *Nucl. Phys.* **A763** (2005) 59.

[14] K. Hebeler et al, *Phys. Rev.* **C83** (2011) 031301.

[15] R. Roth et al., *Phys. Rev.* **C73** (2006) 044312.

[16] J.W. Negele and D. Vautherin, *Phys. Rev.* **C5** (1972) 1472.

[17] B. Gebremariam, T. Duguet and S.K. Bogner, *Phys. Rev.* **C82** (2010) 014305.

[18] N. Kaiser and W. Weise, *Nucl. Phys.* **A836** (2010) 256.

[19] B. Gebremariam, S.K. Bogner and T. Duguet, *Nucl. Phys.* **A851** (2011) 17.

[20] M. Stoitsov et al., *Phys. Rev.* **C82** (2010) 054307.

[21] R. Machleidt and D.R. Entem, *Phys. Reports* **503** (2011) 1.

[22] L. Coraggio et al., *Phys. Rev.* **C75** (2007) 024311.

[23] A. Nogga, S.K. Bogner and A. Schwenk, *Phys. Rev.* **C70** (2004) 061002.

[24] N. Kaiser, *Phys. Rev.* **C65** (2002) 017001.

[25] E. Epelbaum, W. Glöckle and Ulf-G. Meißner, *Nucl. Phys.* **A747** (2005) 362.

[26] J. Fujita and H. Miyawawa, *Prog. Theor. Phys.* **17** (1957) 366.

[27] J.W. Holt, N. Kaiser and W. Weise, nucl-th/1106.5702.